Final Draft August 29, 2023
Typeset using LaTeX **twocolumn** style in AASTeX63

Determining The Dynamical State of XCLASS Galaxy Clusters At Redshift Z < 0.12

Edgar Perez Vidal[1]

[1]*Department of Astronomy, University of California, Berkeley, CA 94720-3411, USA*

ABSTRACT

The cosmic web is a fundamental framework that describes the large-scale structure of the universe, composed of filaments, nodes, and voids, interwoven in a complex network. This work explores the significance of X-ray clusters in reconstructing the cosmic web using galaxy clusters from the Sloan Digital Sky Survey (SDSS). X-ray clusters, immense agglomerations of galaxies and hot gas are pivotal in tracing the distribution of matter and unveiling the underlying structure. By detecting the X-ray emissions from the superheated gas within these clusters, astronomers gain insight into their gravitational interactions and the cosmic environment they inhabit. The dynamical state of X-ray clusters offers vital clues for constructing a comprehensive map of the cosmic web. Advanced telescopes, such as Chandra X-ray Observatory, have enabled the identification and analysis of X-ray clusters and with the successful launch of Euclid, we will further enhance our understanding of the universe's architecture. The following work will summarize the work done under Florian Sarron and Nicolas Clerc at the Institut de Recherche en Astrophysique et Planétologie (IRAP).

1. INTRODUCTION

This study centers on the examination of the cosmic web—the sprawling framework that shapes the universe on a grand scale. Prior to my internship at the IRAP, my understanding of the cosmic web was largely informed by N-body simulations, which delve into the evolution of galaxies within dark matter-dominated environments. Additionally, expensive simulations that include baryonic matter, or hydrodynamic simulations such as the Eagle Project, provide insights into the universe's evolution Schaye et al. (2015).

However, this work hones in on empirical observations for the cosmic web's reconstruction. This entails gathering imagery from the Sloan Digital Sky Survey and employing DisPerSe, a topological algorithm, to generate the universe's skeletal structure Kraljic et al. (2020). Notably, this skeletal output features critical points—local maxima and saddle points—while the links between these critical points manifest as filaments. Hence, leveraging observational data, a successfully reconstructed cosmic web set the stage for a comparative analysis of observed attributes against simulation outcomes.

2. ANALYSIS

Corresponding author: Edgar Perez Vidal
e.vidal8392@berkeley.edu

A crucial lesson I gleaned during this experience was the significance of data visualization. My tasks involved handling three primary datasets: the Tempel Catalogue, the XCLASS Survey, and the skeletal structure extracted using DisPerSe. The Tempel Catalogue aggregates galaxy groups and clusters, assembled by the SDSS and unveiled in DR8 Tempel et al. (2012). Notably, the bulk of this catalog does not pertain to the scope of this study.

On the other hand, the XCLASS Survey encompasses sources emitting x-rays - a product of the elevated temperatures within inter-cluster mediums as galaxies form into clusters, inducing x-ray emissions Ridl et al. (2017).

Given the x-ray emission's positional information, we can identify the associated galaxy cluster and proceed to reconstruct the encompassing cosmic web. Our initial attempt involved a straightforward cross-matching algorithm between catalogs; however, a glaring discrepancy emerged. As illustrated in Figure 1, the center of the x-ray emission and the location of the nearest matched galaxy fail to coincide. Ideally, both of these markers should align, along with the corresponding node in the skeleton. However, it is evident that an issue exists within the catalog matching process. Consequently, we developed a more sophisticated methodology for aligning the x-ray emission with the respective galaxy cluster.

2.1. *Cross Matching Catalogues*

The XCLASS catalog includes entries with redshifts truncated to 3 decimal places, whereas the redshifts in

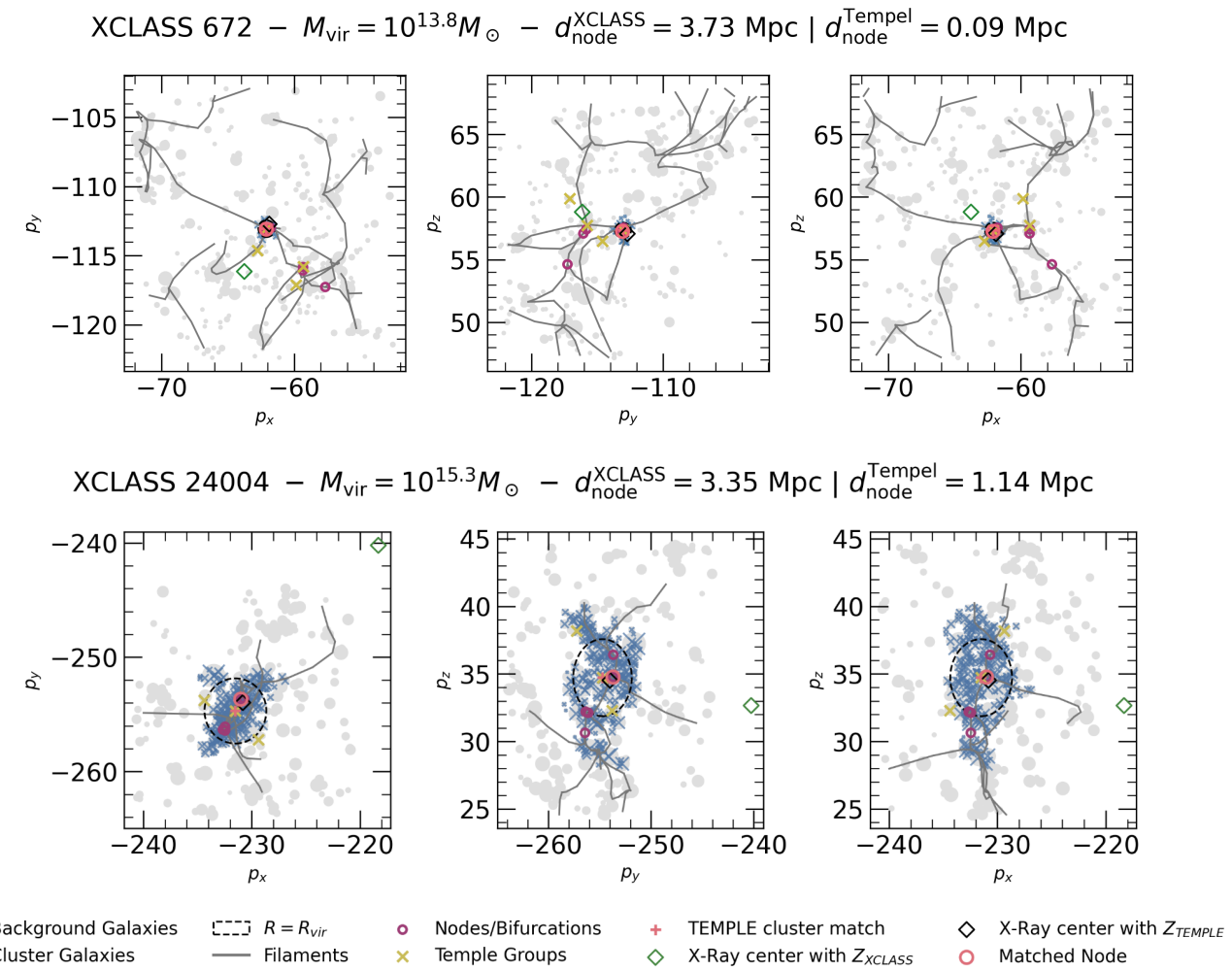

Figure 1. Cartesian View of XCLASS Sample This figure illustrates the Cartesian projection of the XCLASS clusters, aligned via a 'matching' procedure involving the Tempel galaxy node and the nearest node within the skeleton. The alignment of the catalogs was orchestrated utilizing an astropy function, hinging upon redshift data sourced from the XCLASS catalog—a parameter that merits scrutiny due to its inherent uncertainty. The challenge arises from the ambiguous nature of Z_{XCLASS}, resulting in a node-to-node alignment between the skeleton and the corresponding galaxy cluster from the Tempel groups that falls short of the anticipated synchronization. This incongruence provides means to find an alternative method for achieving a more accurate alignment and catalog matching procedure.

the Tempel catalog have been corrected to 5 decimal positions. As a result, the initial cross-matching based on redshift led to matches that deviated by several megaparsecs from what we deemed to be the accurate match. In order to identify the genuine matches, we employed a celestial cylinder defined by a radius of $2R_{\rm fit}$ (corresponding to the extent of the x-ray emission) and a height dz. In line with the scope of this study, an assumption of a 10% error in the reported XCLASS redshift was adopted. Accordingly, we set dz = $Z_{\rm xclass}$ / 10, affording us a 3-dimensional volume for each x-ray emission.

The Tempel catalog encompasses both galaxy clusters and individual galaxies. Accordingly, we opted to isolate all the galaxies that resided within our designated celestial cylinder. However, this approach frequently furnishes multiple potential candidates, prompting the consideration of several strategies to identify the accurate match. One approach involves examining the Cartesian projection of the x-ray emission in conjunction with the distribution of galaxy clusters. It is important to acknowledge that due to the uncertainty of the redshift reported in the XCLASS catalog, we should anticipate a considerable deviation in the p_x projection of the x-ray emission's center.

Examining the celestial diagram is an equally valuable strategy. Often, the x-ray emission aligns directly in front of the brightest cluster galaxy (BCG)—the most luminous and massive galaxy in the cluster. In cases where this alignment is absent, the offset of the x-ray

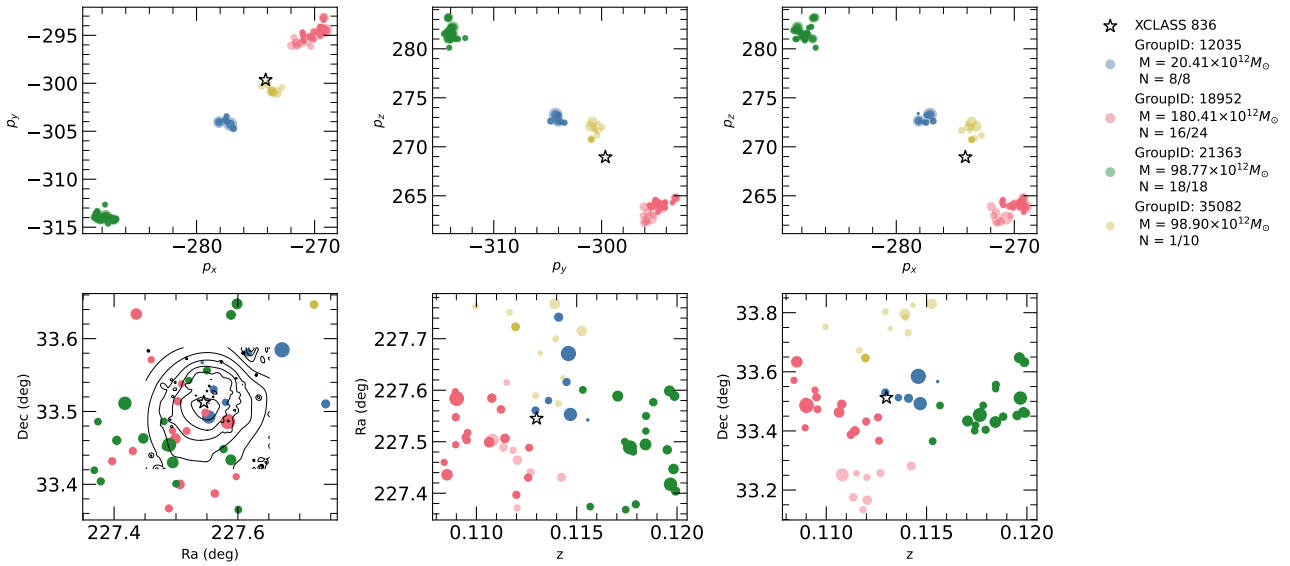

Figure 2. An illustration of our cross-matching algorithm using the case of XCLASS 836. *Top Row:* The top row showcases cartesian projections that visualize the positions of the x-ray emission and the adjoining clusters. Within this visualization, transparent markers indicate background galaxies, while solid markers depict galaxies falling within the confines of the celestial cylinder ($r = 2R_{\rm vir}$ and height dz $\approx 0.1 \times Z_{\rm XCLASS}$). Positioned on the right side of the figure, labels offer insight into the fractions of cluster galaxies contained within the cylinder, along with the corresponding cluster mass. *Bottom Left:* The bottom-left panel provides a celestial perspective, presenting both the x-ray emission and the distribution of galaxies within the cluster. Contour lines of the x-ray emission are superimposed to verify the centering of the x-ray emission. *Bottom middle & right:* Celestial coordinate plots coupled with redshift data, presented separately for Ra and Dec. Through this comprehensive array of visual representations, the figure offers an in-depth exploration of our cross-matching algorithm, with XCLASS 836 serving as a concrete example.

emission may be attributed to active galactic nuclei emitting significant x-ray radiation.

Lastly, cross-referencing the celestial coordinates with the associated redshift provides an additional method for validation. By employing these combined methodologies, we successfully deduced accurate redshift values for 86 clusters, opting to utilize the redshift reported by Tempel when scrutinizing sources from XCLASS. The process of aligning the XCLASS catalog with the Tempel galaxy group is outlined in Figure 2.

3. RESULTS

3.1. *Connectivity*

Having curated a selection of 86 galaxy clusters with rectified redshift values, our focus shifts to exploring the attributes associated with the cosmic web. We proceeded to identify the nearest node within the skeletal structure and establish correlations between them. Our aim was to explore the connectivity linking these clusters while concurrently investigating its relationship with cluster mass. Unlike conventional approaches that often center on the Brightest Cluster Galaxy (BCG), this study exercises diligence by encompassing all galaxies in the cluster.

The concept of connectivity pertains to the number of filaments connecting to a given node. We employed a distance of 1.5 $\times R_{\rm vir}$—a distance where the virial theorem's validity remains intact - to determine the filament count. Prior studies have examined this relationship and showcased a positive correlation between connectivity and cluster mass, as observed in Figure 8 of Malavasi et al. (2023), albeit with some inherent noise.

Within this study, we unveil the correlation existing between connectivity and cluster mass for clusters at redshifts Z < 0.12. Employing Bayesian inference, we determined that the slope of this correlation significantly deviates from zero. In our analysis of the 86 selected samples, we calculated the connectivity while making certain not to overcount supplementary filaments stemming from bifurcation points. This outcome is vividly depicted in Figure 3, wherein the data is binned to display the underlying trend. We implemented a Markov Chain Monte Carlo (MCMC) fit, assuming the linear model expressed as:

$$\kappa = A \log_{10}(M_{NFW}) + B + \sigma_{int} \quad (1)$$

Here, κ denotes the connectivity, M_{NFW} stands for the cluster mass, and A and B represent the slope and intercept, respectively, in suitable units. Additionally,

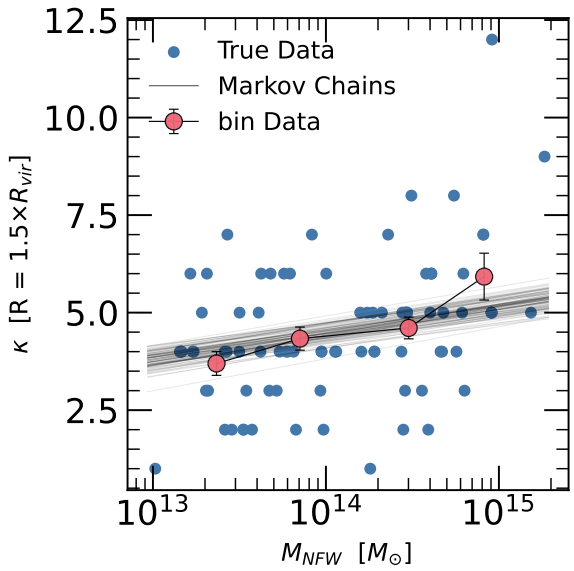

Figure 3. Connectivity vs Cluster Mass The dataset is depicted with blue points, reflecting the actual connectivity values of 86 clusters after rectifying their redshifts. In contrast, the red points illustrate a binned representation wherein the data has been organized based on equal intervals of mass. These red points signify the bin averages of connectivity, and their error bars symbolize the associated standard deviations. In addition, select Markov chains from the MCMC sampling have been superimposed onto the plot, showcasing the underlying correlation, albeit with considerable scatter.

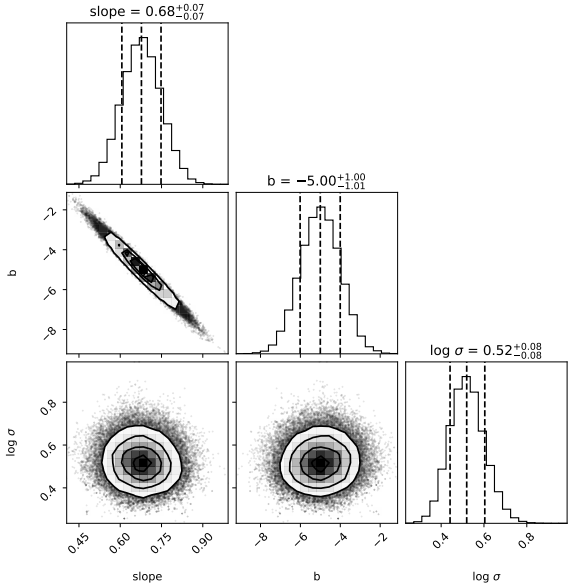

Figure 4. MCMC Results Displayed above are the posteriors, revealing a pronounced correlation between the slope and intercept, wherein the slope demonstrates statistical significance by being notably greater than zero. Our MCMC included a $\sigma_{\rm scatter}$ that fit the intrinsic scatter

σ serves as the nuisance parameter encapsulating the dispersion of the fit. While the fit showcases inherent noise, a statistically significant positive correlation does manifest. Details pertaining to the Markov Chains and posteriors are depicted in Figure 4.

Moving forward, our investigation delved into comprehending the dynamical state of our cluster samples. This entailed quantifying the separation distance from the node within the skeleton to the Brightest Cluster Galaxy (BCG). We implement the definition that systems exhibiting shorter separations are indicative of relaxation, while those with larger separations are deemed perturbed. Employing this criterion, we charted the distribution of these separations and identified two distinctive clusters when observed in logarithmic space. Subsequently, we categorized the clusters with smaller separation distances as relaxed groups and those with larger distances as disturbed groups. Given the substantial time span required for a disturbed state to transition into relaxation, we can confidently infer that all clusters with small separations are indeed in a relaxed state.

Evident from the analysis are two discernible clusters, as depicted in Figure 5. This visual representation not only portrays the distribution of separations but also highlights the dimensionless distribution achieved through division by $R_{\rm vir}$.

Prior to conducting any comparisons between the two groups, our primary concern was to establish the comparability of the galaxies under examination. Within the framework of this study, a fundamental objective was to ensure that the redshift distribution between the disturbed and relaxed galaxies was sufficiently analogous to enable meaningful comparisons. A more pronounced equivalence in redshift becomes apparent, particularly in the context of dimensionless parameterization as shown in the bottom right panel of Fig. 5.

Using the dimensionless parameterization, we wanted to see if there was a correlation to the connectivity between disturbed and relaxed clusters. It appears that there is no statistically significant correlation greater than 2σ as shown in Fig. 6.

4. DISCUSSION

A perplexity that arose was the absence of a more pronounced correlation between connectivity and the dynamical state. Consider the instance of the Bullet cluster, postulated to have formed from the collision of two clusters. It would be reasonable to anticipate that prior to the collision, these clusters were interconnected by

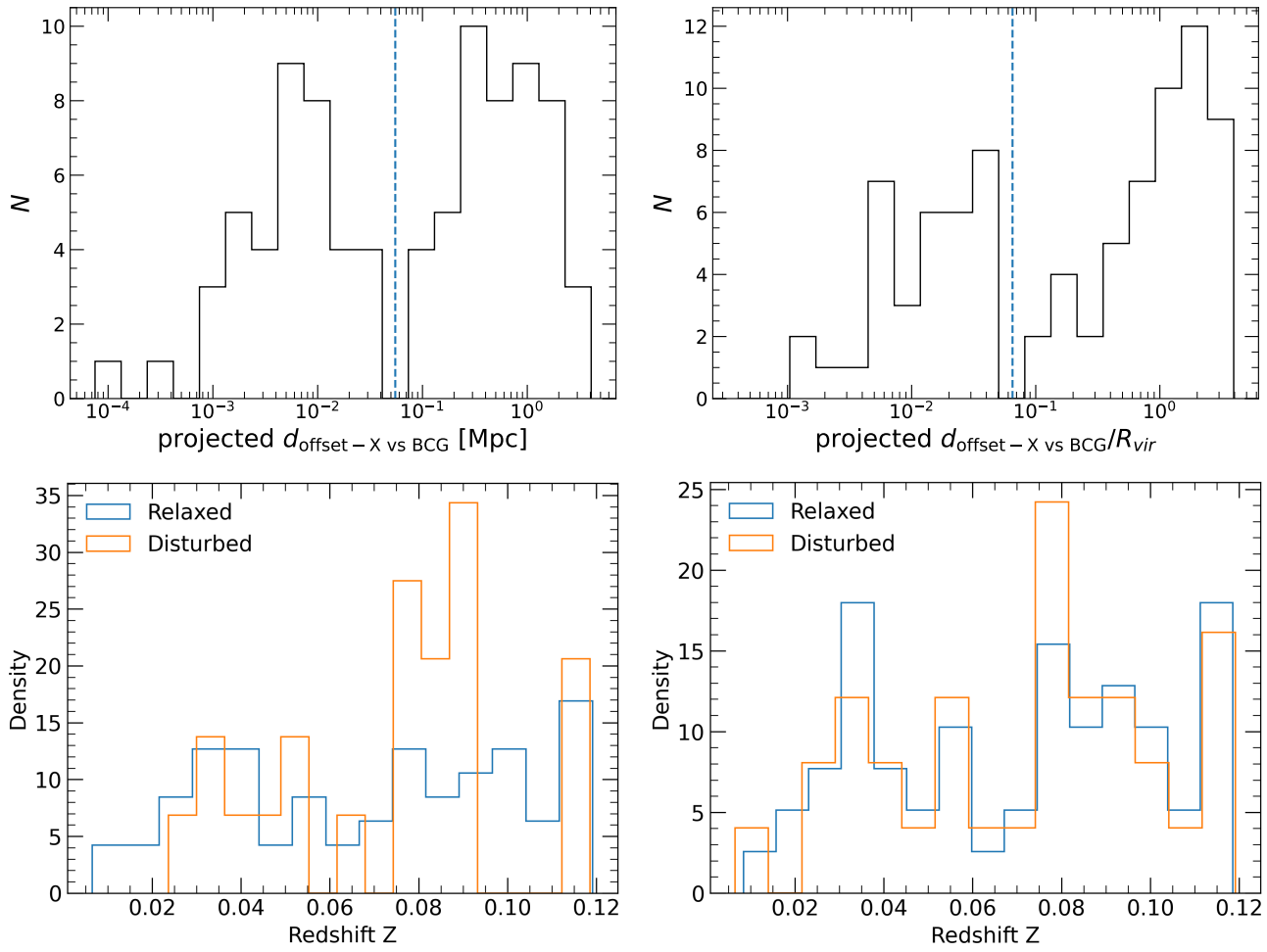

Figure 5. Separation Between X-ray Emission and BCG *Top Row:* We calculated the projected distance between the x-ray emission, utilizing the revised redshift, and the Brightest Cluster Galaxy. The dashed blue line represents the threshold distance for distinguishing between relaxed and disturbed states, wherein relaxed states exhibit separations smaller than disturbed states. *Bottom Row:* The distribution of redshifts among relaxed and disturbed clusters is displayed. The utilization of dimensionless parameterization facilitates a more comparable comparison between the two distinct dynamical states.

a certain number of filaments. However, post-collision, the expected outcome would involve the summation of filament connections. Notably, there's no apparent reason to assume that filaments would collide and collapse, especially given our understanding that filaments mainly comprise dark matter—devoid of pressure and devoid of interaction with light. This leads me to believe that the filaments would merely pass by each other, analogous to how galaxies interact during collisions. There must be some underlying assumption made when determining the dynamical state.

A more comprehensive strategy involves a direct examination of the x-ray images. Specifically, valuable insights about the dynamical state can be gleaned from understanding the concentration and centroid shift of the x-ray emission Lovisari et al. (2017). Various morphologies of x-ray emission offer distinct indications of the dynamical state, presenting a more promising avenue for making comparisons and potentially restoring the correlation between dynamical state and connectivity.

This aspect of the project was more exploration-based as it was my first time working with x-ray images, which also involved acquainting myself with the poison noise. Throughout this exploration, I acquired techniques like image smoothing through the addition of Gaussian noise, which results in improved visual representation. This enhancement is particularly significant due to the inherent nature of x-ray observations, where discrete photon collection is associated with a certain probability, hense the poison noise. I see some applications of machine learning and deep learning here.

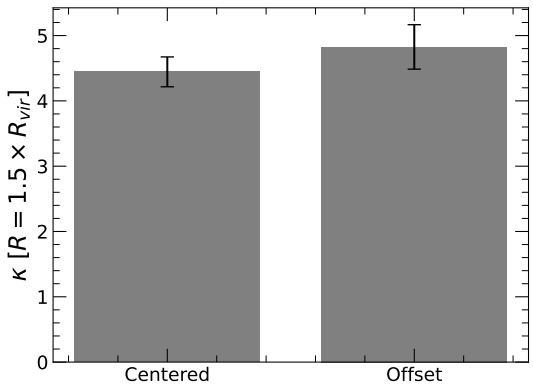

Figure 6. Connectivity of Disturbed and Relaxed clusters. Employing dimensionless parameterization for the projected distance between the x-ray emission and the BCG, we computed the average connectivity along with its standard deviation between the different dynamical states. Center and offset refer to relaxed and disturbed states respectively. Our expectation was to observe a difference exceeding 2 σ to establish statistical significance; however, the current findings do not align with this criterion.

Perhaps a score-based model (diffusion model) could be trained on high signal-to-noise images, adding non-gaussian noise to recreate the poison noise and the systemic noise from the instruments, which can take an input x-ray image and output a smooth image with greater detail.

5. CONCLUSION

Throughout my 10 weeks at the IRAP, I got the opportunity to hone my computation skills and explore a new topic in Astrophysics. I participated in a few GAHEC talks which exposed me to possible research topics to pursue for my graduate studies. I summarize my work at the IRAP as follows:

- Explored the cosmic web by aligning XCLASS clusters with Tempel galaxy nodes and skeleton nodes.
- Employed an advanced cross-matching approach to account for deviations in the alignment.
- Managed uncertainties in XCLASS redshifts by adopting Tempel catalog's more accurate redshifts.
- Investigated the connectivity between clusters, considering filament interconnections.
- Leveraged Bayesian inference to examine the correlation between connectivity and cluster mass.
- Demonstrated a statistically significant correlation with cluster mass despite inherent noise.
- Analyzed the separation between skeleton nodes and Brightest Cluster Galaxies (BCGs) for dynamic state evaluation..
- Concluded that clusters with small separations are in a relaxed state, given the prolonged timescales for transitioning from a disturbed to a relaxed state.
- Began exploring the dynamical state using X-Ray images.

Facilities: SDDS, XMM-Newton, Chandra

Software: Python Jupiter Notebook, Numpy, PYMC, Astropy, Matplotlib, Pandas, Scipy

ACKNOWLEDGMENTS

E.P.V would like to express gratitude to the Les Minorités Importente program, facilitated by the International Center of Excellence NSF (NICE), for the invaluable opportunity to participate in a summer research experience at the Université de Toulouse, Paul Sabatier. This work would not have been feasible without the generous funding from the CAL Nerds program hosted at the University of California, Berkeley. E.P.V would also like to extend appreciation to Florian Sarron, Ph.D, and Nicolas Clerc, Ph.D, for their invaluable mentorship at IRAP.

REFERENCES

Kraljic, K., Pichon, C., Codis, S., et al. 2020, Monthly Notices of the Royal Astronomical Society, 491, 4294

Lovisari, L., Forman, W. R., Jones, C., et al. 2017, The Astrophysical Journal, 846, 51

Malavasi, N., Sorce, J. G., Dolag, K., & Aghanim, N. 2023, arXiv preprint arXiv:2306.03124

Ridl, J., Clerc, N., Sadibekova, T., et al. 2017, Monthly Notices of the Royal Astronomical Society, 468, 662

Schaye, J., Crain, R. A., Bower, R. G., et al. 2015, Monthly Notices of the Royal Astronomical Society, 446, 521

Tempel, E., Tago, E., & Liivamägi, L. 2012, Astronomy & Astrophysics, 540, A106